Delft University of Technology

Interaction of carbon partitioning, carbide precipitation and bainite formation during the Q&P process in a low C steel

Hajy Akbary, F; Sietsma, J; Miyamoto, G; Furuhara, T; Santofimia, MJ

Important note
To cite this publication, please use the final published version (if applicable).
Please check the document version above.

Full length article

Interaction of carbon partitioning, carbide precipitation and bainite formation during the Q&P process in a low C steel

Farideh HajyAkbary [a, b, *], Jilt Sietsma [b], Goro Miyamoto [c], Tadashi Furuhara [c], Maria Jesus Santofimia [b]

[a] Materials Innovation Institute (M2i), Delft, The Netherlands
[b] Delft University of Technology, Delft, The Netherlands
[c] Institute for Materials Research, Tohoku University, Japan

ARTICLE INFO

ABSTRACT

Theoretical understanding of the "quenching and partitioning" (Q&P) process allowed developing microstructures consisting of carbon-depleted martensite and retained austenite that deliver superior mechanical properties. Most of the models describing the Q&P process are limited to systems in which carbide precipitation in martensite and decomposition of austenite to bainite are totally suppressed. However, these reactions are often unavoidable, even in low-carbon steels containing a relatively high concentration of Si and Mn. This work investigates interactions between carbon partitioning, carbide precipitation and carbide-free bainite formation during the Q&P process of a 0.3C–1.6Si–3.5Mn (wt.%) steel with non-homogenous distribution of the alloying elements. It was found that prior to the partitioning step ε-carbide forms in martensite. The decomposition of this carbide is required for a full completion of the carbon partitioning from martensite to austenite. Slow kinetics of decomposition of ε-carbide retards the carbon partitioning process. Results show that a fraction of austenite becomes stable by carbon partitioning and does not decompose to bainite. In the specimens quenched to lower temperature, a higher fraction of austenite becomes stable and consequently a lower fraction of bainite is formed.

1. Introduction

The "quenching and partitioning" (Q&P) process is known as a promising method for developing steels with good combinations of strength and ductility [1]. The Q&P process involves rapid quenching of an austenitic microstructure to a temperature lower than the martensite-start temperature (M_s) to form a controlled fraction of initial martensite (M_1). Then, the treatment is followed by isothermal holding either at or above the initial quenching temperature to stabilize austenite via carbon partitioning from supersaturated martensite to austenite. The Q&P process is ended by quenching the microstructure to room temperature during which some secondary martensite (M_2) may form if the carbon

enrichment is not sufficient to stabilize all austenite [2]. Secondary martensite contains a high concentration of carbon and is detrimental for ductility [3]. Formation of M_2 can be controlled by knowledge of the carbon partitioning process as well as its interactions with other possible reactions such as martensite-austenite interface migration, carbide precipitation in martensite and decomposition of austenite to bainite.

The thermodynamics of the carbon partitioning process can be well described on the basis of "constrained carbon equilibrium" (CCE) [4,5]. In this approach, the partitioning process across an immobile austenite-martensite interface is ended when martensite (i.e. ferrite) is in metastable equilibrium with austenite. Santofimia et al. [6] adapted the model to simulate the interaction between the carbon partitioning and the possible migration of martensite-austenite interfaces. These approaches are limited to well-controlled systems in which carbide precipitation in martensite and decomposition of austenite to bainite are totally suppressed. However, these reactions are often unavoidable, even in low-carbon steels containing a relatively high concentration of Mn

and Si [7–9].

Precipitation of ε-carbide prior to the partitioning step or of cementite during the isothermal holding affects the carbon partitioning process. Precipitation of cementite reduces the amount of carbon in solid solution in martensite and therefore decreases the degree of carbon enrichment that can be reached in austenite [10,11]. Generally, a high concentration of Si is added to the steel composition to control cementite formation [12]. However, Si improves the coherency at the carbide-martensite interface during the nucleation stage of the ε-carbides [13] and consequently increases the stability of the ε-carbides [2,13,14]. Consequently, suppressing precipitation of ε-carbide is really challenging and practical designing of Q&P treatments requires knowledge of the interaction between ε-carbide precipitation and carbon partitioning process.

The carbon partitioning process may also overlap with the decomposition of austenite to bainite. Formation of carbide-free bainite associates with carbon enrichment of austenite and could stabilize austenite. Therefore, bainite formation has an important influence on the final microstructure. Developing a model that indicates the interaction between bainite formation and carbon partitioning process assists in better controlling the microstructure.

In this paper, the microstructural evolution during the Q&P process of a 0.3C-1.6Si-3.5Mn (wt.%) steel with non-homogenous chemical composition is analysed. The influence of the carbide precipitation as well as the formation of carbide-free bainite on the microstructure is discussed based on experimental observations and microstructural modelling.

2. Experimental procedures

Cylindrical specimens with length of 10 mm and diameter of 3.5 mm were machined parallel to the hot-rolling direction of 0.3C−1.6Si−3.5Mn (wt.%) steel sheets. A scheme of the applied heat treatments is shown in Fig. 1. The specimens were austenitized at 900 °C for 180 s, quenched to 180 °C, 200 °C, 220 °C, 240 °C and 260 °C, isothermally treated at 400 °C for 5 s, 10 s, 50 s, 100 s and 200 s and finally quenched to room temperature in a Bähr DIL 805 A/D dilatometer. In this paper, the code QTxxx-y identifies the specimen that was quenched to xxx °C and isothermally treated at 400 °C for y seconds. In addition to the Q&P specimens, one "as-quenched" specimen was created by austenitization at 900 °C for 180 s and then directly quenched to room temperature.

After conventional metallographic preparation, specimens were etched with 2% Nital for subsequent optical microscopy and scanning electron microscopy (SEM) observations using a JEOL JSM-6500F field emission gun scanning electron microscope (FEG-

SEM) operating at 15 kV. The specimens were metallographically prepared for electron backscatter diffraction (EBSD) examination with a final polishing step of 0.05 μm using an OPS suspension for 1 h. The analyses were done by orientation imaging microscopy (OIM) on a FEI Nova 600 Nanolab dual-beam (focused ion beam) FEG-SEM, under the following conditions: acceleration voltage 20 kV; working distance 25 mm; tilt angle 70°; step size 50 nm. The orientation data were post-processed with the TSL system. Furthermore, selected specimens were observed with a transmission electron microscope (TEM; Philips CM300) operated at 300 kV. Thin-foils of TEM were prepared by twin-jet electro-polishing at 25−30 V in solution of 10% HClO$_4$ in ethanol at room temperature. Distributions of Mn and Si in selected regions were analysed using electron probe micro analyzer (EPMA) technique. EPMA measurements were performed with a JEOL JXA 8900R microprobe using a 10 keV electron beam with beam current of 50 nA employing wavelength-dispersive spectrometry (WDS).

Volume fractions of RA (f^{RA}) as well as carbon concentration of RA (X_C^{RA}) were determined by means of X-ray diffraction (XRD) analysis using a Bruker type D8-Advance diffractometer, in a 2θ range from 30° to 135°, with Co Kα radiation. The calculation of f^{RA} and X_C^{RA} was performed in accordance with the method given in Ref. [15]. Volume fractions of initial martensite (f^{M1}), formed during the initial quench, bainite (f^B), formed during the isothermal holding, and secondary martensite (f^{M2}), formed during the final quench, were evaluated by applying the lever rule on the dilatometer data. In order to provide accurate values of the thermal expansion coefficients of austenite and martensite for the lever rule method, an as-received specimen was heated to 900 °C and then quenched to room temperature. The treatment was followed by reheating the specimen to 900 °C and finally quenching to room temperature. Thermal expansion coefficients of austenite and martensite were determined from the data during the first quenching and the second heating process, respectively. Considering that f^{RA} in the as-quenched specimen is lower than the detection limit of the XRD measurements (0.02), it can be assumed that the microstructure during the second heating was fully martensitic and dilatometry data provides thermal expansion coefficient of martensite. For each specimen, f^{RA} was determined by subtracting volume fractions of bainite, M_1 and M_2 (which were calculated from the lever rule) from unity and compared with the value that was measured by XRD analysis. There was a difference about ±0.02 between f^{RA} which was determined from the lever rule and the ones measured from XRD and therefore this value is considered as the uncertainty of the lever rule measurements.

3. Results

3.1. Analysis of compositional gradients in the steel

Fig. 2a shows an optical micrograph of the specimen QT260-5. The microstructure consists of internally etched features, M_1, and blocky white features, M_2, which are distributed forming bands. In this specimen, as in the other Q&P specimens, microstructural bands are parallel to the rolling direction. This shows non-homogeneous distribution of the alloying elements in the transverse direction. Concentrations of Mn and Si along the transverse direction, the black arrow in Fig. 2a, were determined by EPMA and the results are illustrated in Fig. 2b. Concentrations of Mn and Si fluctuate between 2.9 and 4.2 wt.% and 1.1−1.6 wt.%, respectively. Non-homogeneous distribution of the Mn and Si is caused by the rejection of these elements to the inter-dendritic spaces during the solidification process. According to Fig. 2a and b, the fraction of M_1 is higher in the low-solute regions and the fraction of M_2 is higher in the high-solute regions.
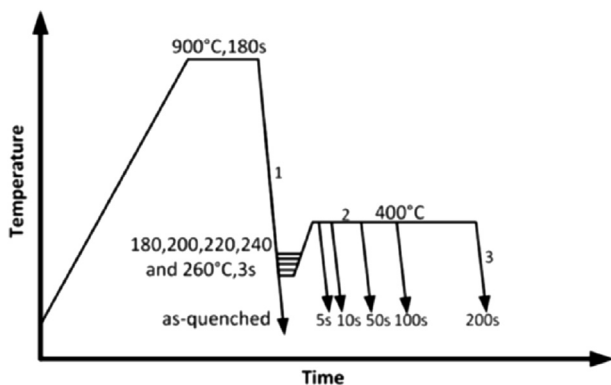

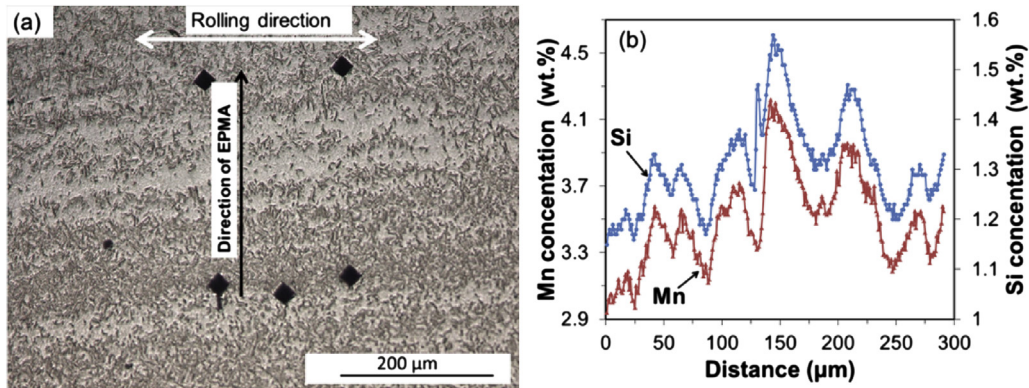Fig. 1. Scheme of the heat treatments.

Fig. 2. (a) Optical micrograph of the specimen QT260-5 and (b) distribution of Mn and Si along the black arrow in Fig. 2a.

Regarding the fact that Mn lowers the chemical potential of carbon in austenite, it is expected that high-Mn regions attract carbon. The influence of Mn segregation on carbon concentration is determined by ThermoCalc, using TCFE7 data base. This was done by determining the equilibrium carbon concentration at the austenitization temperature (900 °C) while varying the Mn concentration. In these calculations, Mn concentration varies in the range of 2.9–4.2 wt.% with a step of 0.25 wt.% and the concentration of Si is considered fixed (1.6 wt.%). According to the calculations, increasing Mn concentration from 2.9 wt.% to 4.2 wt.% increases the carbon concentration from 0.29 wt.% to 0.31 wt.%.

3.2. Microstructural observations

Figs. 3a–d shows SEM micrographs of the as-quenched, QT180-5, QT180-200 and QT260-5 microstructures, respectively. The as-quenched specimen consists of martensite and carbides. The Q&P specimens are composed of internally etched features, M_1, blocky features, M_2, and thin films of RA. Precipitation of carbides inside M_1 grains is evident. For each quenching temperature, increasing the isothermal holding time decreases the fraction carbide and consequently increases the fraction of carbide depleted M_1 grains, as it is shown in the specimens QT180-5 and QT180-200 in Fig. 3b and c, respectively.

Fig. 4a and b shows bright filed images of the specimens QT180-5 and QT180-200, respectively. The carbide type was identified by selected area diffraction (SAD) analysis; here only ε-carbide and cementite were considered. Fig. 4c illustrates SAD pattern and Fig. 4d the ideal SAD pattern corresponding to the bright field image of the specimen QT180-200. Table 1 compares the calculated
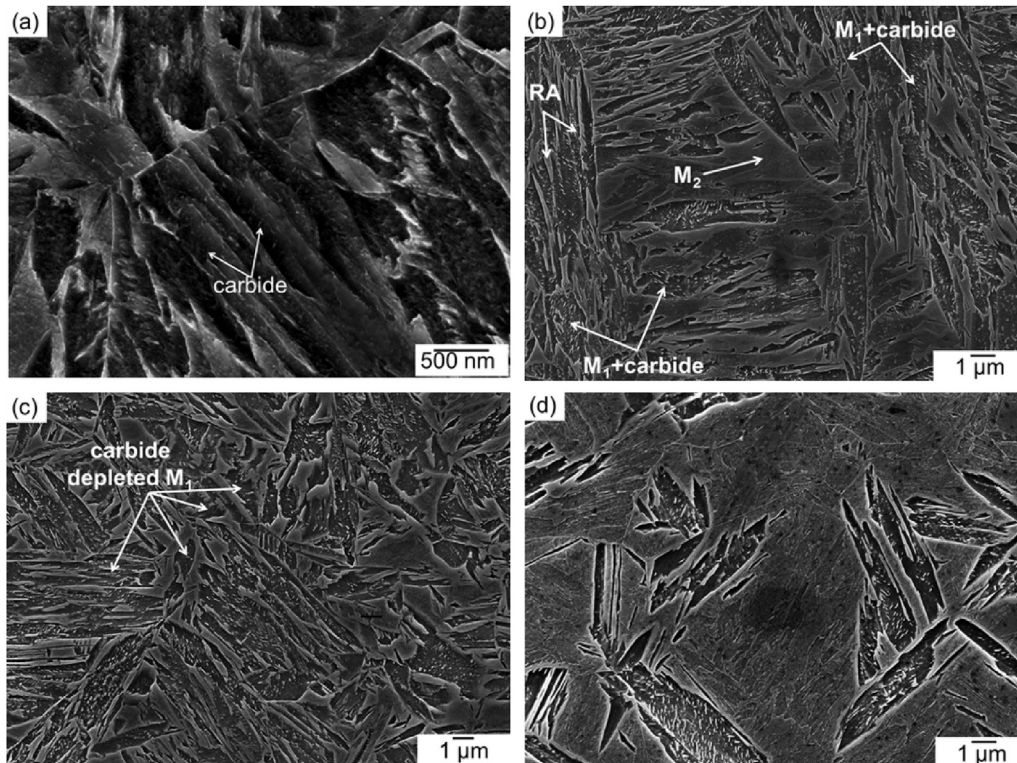

Fig. 3. SEM micrograph of the specimens (a) as-quenched, (b) QT180-5, (c) QT180-200 and (d) QT260-5. M_1 is initial martensite, RA is retained austenite and M_2 is secondary martensite.
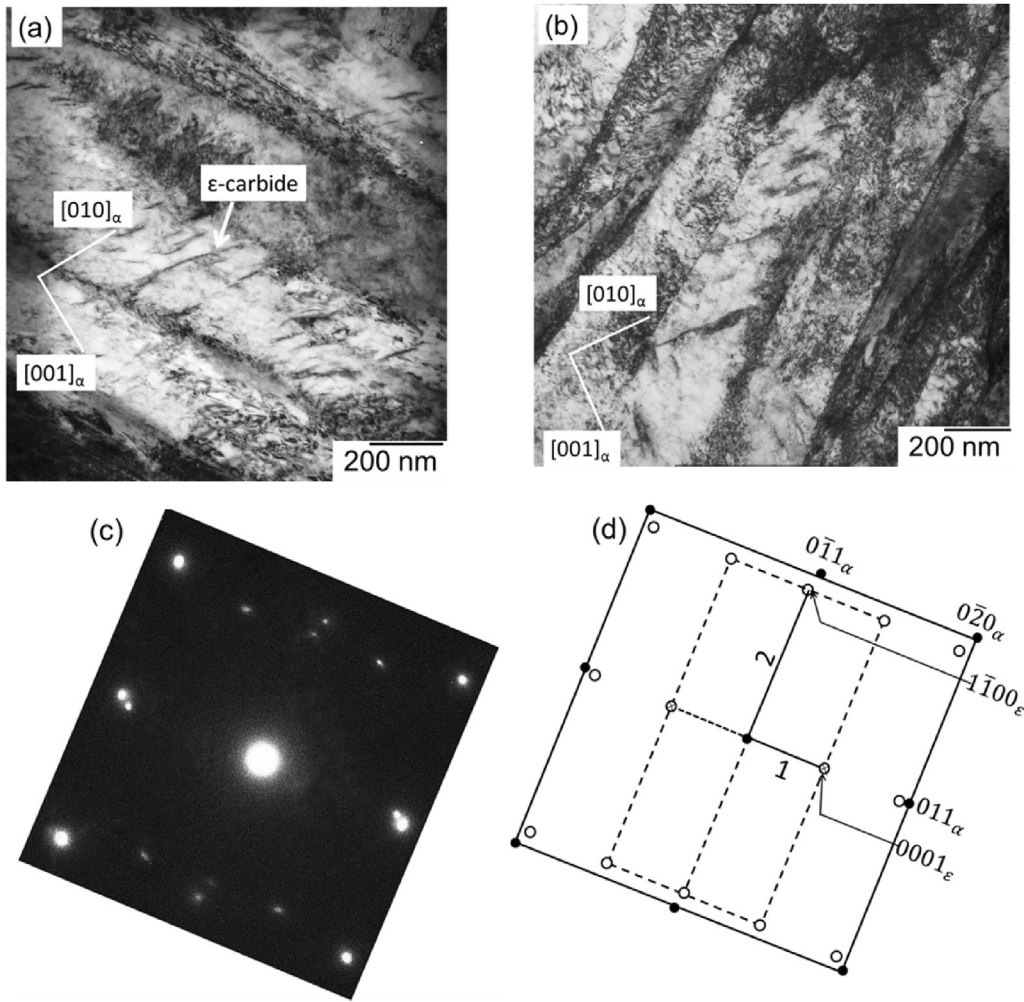
Fig. 4. Bright field micrograph of the specimens (a) QT180-5 and (b) QT180-200, (c) SAD pattern of region shown in Figs. 4b and (d) the corresponding key diagram. Filled circles belong to ferrite reflections and open circles show carbide reflections and open circles with cross show forbidden carbide reflections and beam~//[100]$_\alpha$~//[11$\bar{2}$0]$_\varepsilon$.

Table 1
Comparison between the calculated and experimentally obtained interplanar spacing of line 1 and 2 in Fig. 4c. The *d*-spacing was calculated using the parameters $a = 2.752$ Å, $c = 4.353$ Å for ε−carbide [16] and $a = 4.525$ Å, $b = 5.900$ Å, $c = 6.744$ Å for θ [17].

	Measured interplanar spacing (Å)	Calculated interplanar spacing (Å)	
		ε	θ
1	4.36	$d_{0001} = 4.35$	$d_{011} = 4.06$
2	2.40	$d_{1\bar{1}00} = 2.38$	$d_{200} = 2.26$

and the experimentally obtained interplanar spacing between vector 1 and 2 in Fig. 4c. The measured interplanar spacing is close to the values reported for ε-carbide, which confirms the presence of ε-carbide in the specimens. Comparing dark field images of carbide in six different areas in one QT180-5 specimen and one QT180-200 specimen indicates that the fraction of ε-carbide decreases by increasing the isothermal holding time. Although TEM and SEM are not ideal methods for quantitative determination of the fraction of carbide these techniques can be applied for qualitative comparison of the carbide fraction.

Fig. 5 shows a combined grain average Image Quality (IQ) and phase map of the specimen QT220-5 obtained by EBSD. In this map,

RA grains are shown in green and martensite grains, including M$_1$ and M$_2$, are indicated in red. Due to the higher carbon concentration and dislocation density of M$_2$ with respect for M$_1$, the IQ for M$_2$ grains is lower than of M$_1$ grains [18]. Some M$_2$ grains, dark red grains, are indicated in Fig. 5.

3.3. Modelling of carbon partitioning process

Carbon partitioning from martensite to austenite, at the isothermal holding temperature of 400 °C, is simulated based on the model given in Ref. [6] for a Fe−C system with immobile martensite-austenite interfaces. The model assumes that carbide precipitation and bainite formation do not occur before or during the isothermal holding. The lath width of martensite is assumed independent of the quenching temperature and given as 0.2 μm [19]. The austenite grain size is determined using the "constant-ferrite width" approach [20] as 0.05 μm and 0.8 μm for the specimens QT180 and QT260, respectively, because of the respective austenite fractions at the isothermal holding temperature.

Fig. 6a and b illustrate the evolution of the carbon profile in an austenite grain of the specimens QT180 and QT260, respectively. Based on the simulations, isothermal holding of 1 s is sufficient for complete carbon diffusion from martensite to austenite for all austenite fractions after the quenching. However, 5 s of isothermal
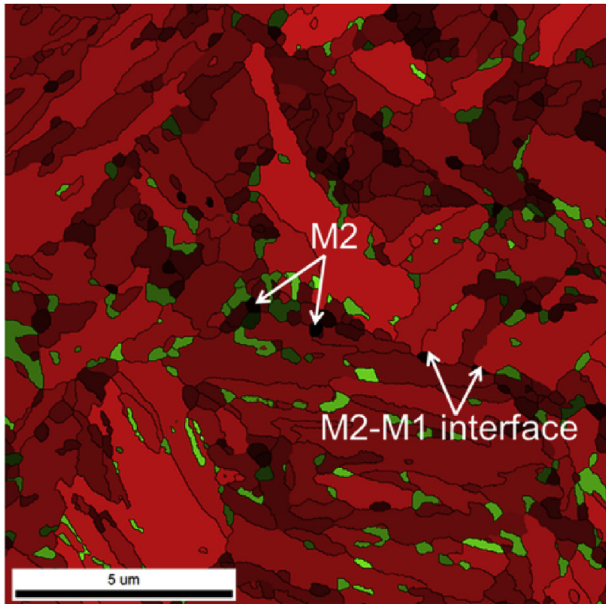
Fig. 5. Combined average grain Image Quality (IQ) and phase map of the specimen QT220-5, in which black boundaries are high angle grain boundaries (misorientation higher than 15°). Martensite and austenite are coded by red and green, respectively. (For interpretation of the references to colour in this figure legend, the reader is referred to the web version of this article.)

holding is sufficient to homogenise carbon inside an austenite grain of the specimen QT180, isothermal holding longer than 200 s is required for the specimen QT260. This results from the low mobility of carbon in austenite and regarding the fact that the austenite grain size of the specimen QT260 is about 16 times of the specimen QT180.

The critical carbon concentration by which austenite becomes stable at room temperature can be determined on the basis of the relation between chemical composition and M_s [21]:

$$M_s = 565 - 600[1 - exp(-0.96X_C)] - 31X_{Mn} - 13X_{si} - 10X_{Cr} - 18X_{Ni} - 12X_{Mo}$$

$$(1)$$

where X_i is the concentration of element i in wt.%. Considering M_s as 25 °C, X_{Mn} as 3.5 wt.% and X_{Si} as 1.6 wt.%, the critical carbon concentration of austenite is given as 1.2 wt.%. Accordingly, austenite with carbon concentration higher than 1.2 wt.% does not

transform to M_2 during the final quenching. By decreasing the carbon concentration of austenite to values lower than 1.2 wt.%, the fraction of austenite which remains at room temperature decreases. Fig. 6a shows that after 5 s of isothermal holding, austenite in the specimen QT180 contains 1.5 wt.% carbon and therefore all austenite retains at room temperature. On the contrary, Fig. 6b shows that a steep carbon gradient from 0.95 wt.% to 0.3 wt.% is observed in the specimen QT260-5. After 200 s of isothermal holding of the specimen QT260, the carbon distribution becomes almost homogeneous within the austenite grain and it reaches an average value of 0.4 wt.%. The carbon concentration of austenite in both the specimens QT260-5 and QT260-200 is below the critical concentration and therefore part of austenite transforms to M_2 during final quenching.

3.4. Volume fractions and carbon content of retained austenite

Volume fractions of RA (f^{RA}) of the Q&P specimens are determined on the basis of XRD analysis and the carbon partitioning simulations. The results are shown in Fig. 7a. A comparison between the calculated and the measured f^{RA} leads to the following observations;

(a) For each partitioning time, the measurements show that the specimens QT200 and QT220 have the highest fraction of RA. Considering the experimental uncertainty, this agrees well with the simulations which give the highest fraction of RA for the specimens QT200.
(b) According to the simulations, increasing the isothermal holding time from 5 s to 200 s does not affect f^{RA} of the specimens QT180 and QT200, while f^{RA} of the specimens QT220, QT240 and QT260 decreases. On the contrary, the measured f^{RA} increases by increasing the isothermal holding time from 5 s to 200 s, being the increase of f^{RA} is more pronounced in the specimens QT220, QT240 and QT260.
(c) For all the quenching temperatures, the simulated f^{RA} of the specimens isothermally held for 5 s is higher than the measured ones. By increasing the isothermal holding time to 200 s, the simulated f^{RA} of the specimens QT180 and QT200 is still higher than the measured ones. However, the simulated f^{RA} of the specimens QT220, QT240 and QT260 is lower than the measured f^{RA}.

Carbon concentrations of RA (X_C^{RA}) are presented in Fig. 7b. The values of X_C^{RA} varies in the range of 0.7 wt.%-1.0 wt.% which is lower than the 1.2 wt.% (according to the carbon partitioning simulation)
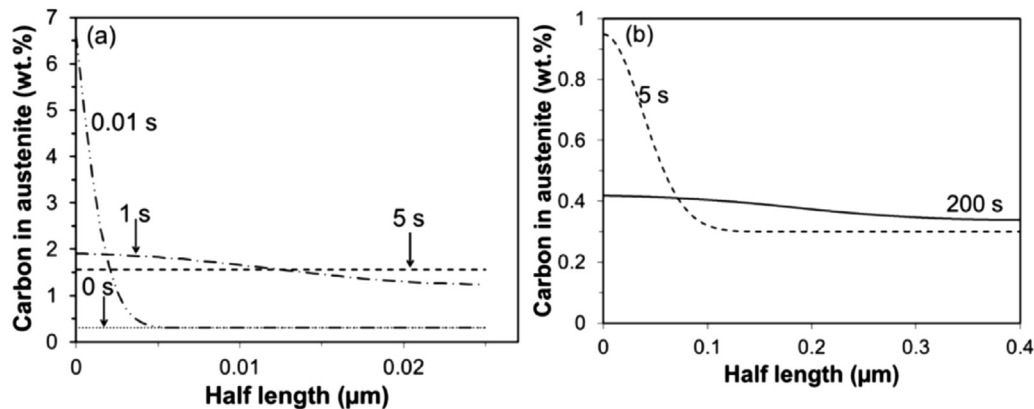

Fig. 6. Evaluation of carbon profile in an austenite grain during isothermal holding of the specimens (a) QT180 and (b) QT260, on the basis of calculations.
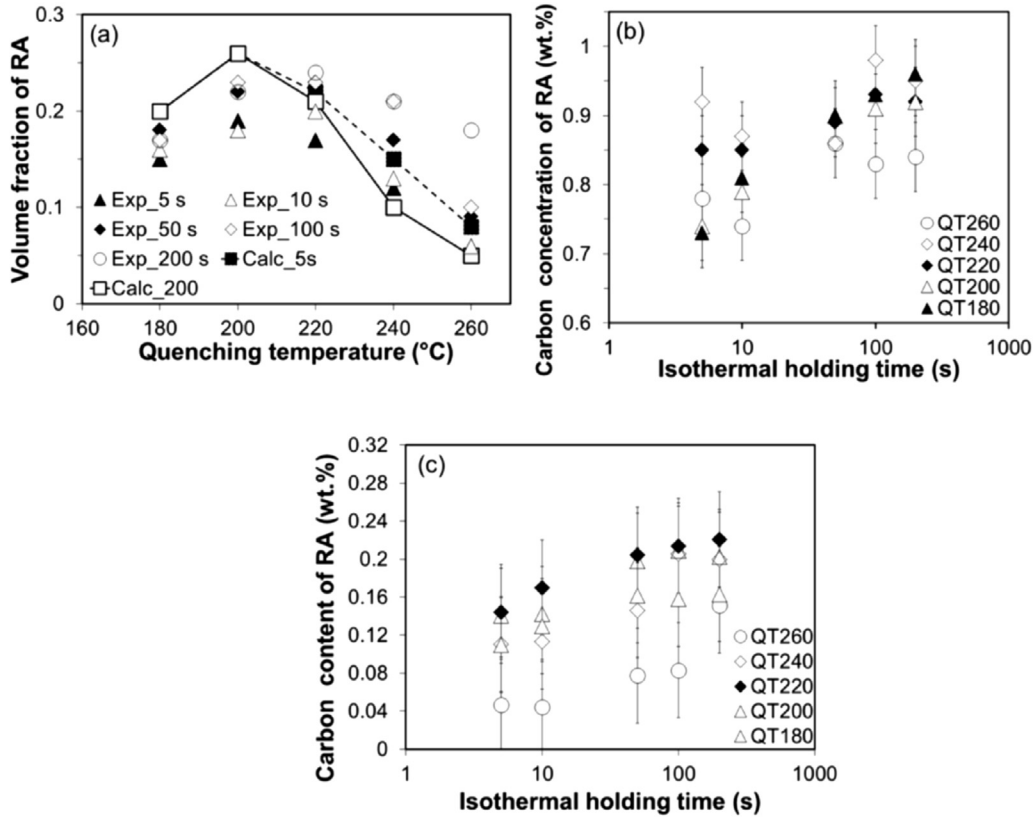
Fig. 7. (a) Calculated (Calc.) and experimentally (Exp.) measured volume fractions of RA as a function of the quenching temperature for the specimens isothermally held at 400 °C for different times. Influence of isothermal holding on (b) carbon concentration in RA (X_C^{RA}) and (c) total carbon content of RA ($C^{RA} = f^{RA} X_C^{RA}$) of the Q&P specimens with different quenching temperatures.

which is required to stabilize all austenite at room temperature. This agrees well with formation of M_2 in the Q&P specimens. No clear trend can be detected in the behaviour of X_C^{RA} of the Q&P specimens as a function of the isothermal holding time and the quenching temperature. Fig. 7c shows the effect of the isothermal holding time on the total carbon content of RA (C^{RA}). Total carbon content for given phase (C^j) is defined as:

$$C^j = f^j X_C^i \tag{2}$$

where f^j and X_C^i are volume fraction and carbon concentration for phase j (j = RA, M_1 and M_2), respectively. The highest C^{RA} in the specimens QT180, QT200 and QT220 is obtained after 50 s of isothermal holding. For the specimens QT240 and QT260, the highest C^{RA} is achieved by 100 s and 200 s of isothermal holding, respectively.

3.5. Dilatometry analysis of the Q&P heat treatments

The Q&P process is divided into three stages that are shown by numbers 1 to 3 in Fig. 1.

Stage 1 (initial quench). The fractions of initial martensite (f^{M1}) that are formed during the initial quenching of the specimens QT180, QT200, QT220, QT240 and QT260 are 0.79, 0.74, 0.65, 0.52 and 0.49, respectively. The fractions of M_1 are determined by applying lever rule and the accuracy of the fraction is ±0.02.

Stage 2 (isothermal holding). Fig. 8a shows the influence of the isothermal holding on the relative length of the Q&P specimens. The increase of the relative length of the specimens during the isothermal holding can be related to the carbon partitioning from martensite to austenite [22] and to decomposition of austenite to

bainite. The former reaction leads to a length increase that is much smaller than measured ones [22] and therefore the total length increase is mainly related to the latter reaction. The fraction of bainite (f^B) is determined by applying the lever rule and the results are shown in Fig. 8b. For the specimens QT180 and QT200, f^B is less than 0.01, which is below the detecting limit. For the specimens QT220, QT240 and QT260, f^B increases till 200 s.

Stage 3 (final quench). The expansion of the Q&P specimens during the final quench is related to the transformation of unstable austenite to M_2. Fig. 9 shows volume fraction of M_2 (f^{M2}) versus isothermal holding time. For the specimens QT180 and QT200, isothermal holding longer than 5 s does not affect f^{M2}. However, f^{M2} of the specimens QT220, QT240 and QT260 decreases when quenching after longer isothermal holding. For a given isothermal holding time, f^{M2} of the specimens QT180 and QT200 are similar, while f^{M2} of the specimens QT220, QT240 and QT260 increase as a results of increasing the quenching temperature.

3.6. Carbon content of secondary martensite

Carbon concentration of M_2 (X_C^{M2}) can be determined by fitting Koistinen and Marburger (KM) equation [23], as:

$$f^{M_2} = 1 - \exp\left(-\alpha_m(T_{KM} - T)\right) \tag{3}$$

to the experimental plot of volume fraction of M_2 (f^{M_2}) vs. quenching temperature (T). In this approach, α_m, the rate parameter, and T_{KM}, the theoretical martensite start temperature, are fitting parameters. Finally, X_C^{M2} is given by the empirical relations between the chemical composition and α_m as well as T_{KM} [24]. This approach is applicable if carbon is homogenously distributed in the
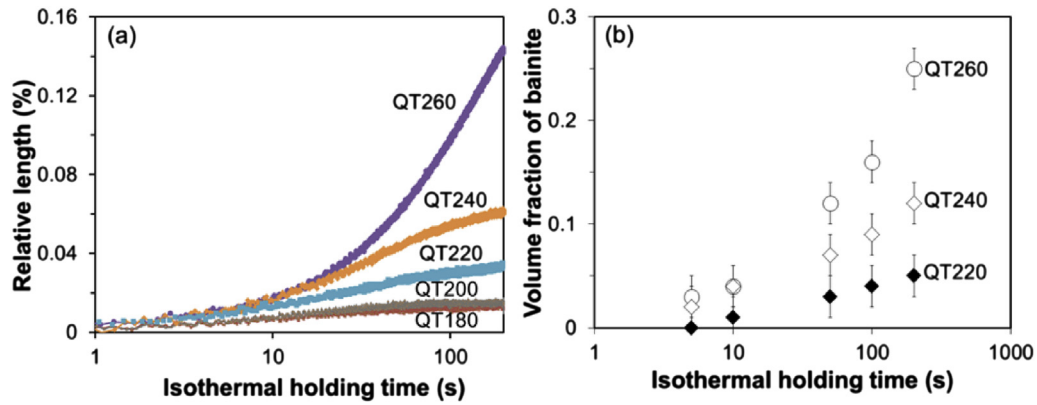
Fig. 8. The influence of the isothermal holding at 400 °C on the (a) relative length change of the Q&P specimens and (b) volume fractions of bainite in the specimens QT220, QT240 and QT260. The fractions of bainite are almost zero in the specimens QT180 and QT200.
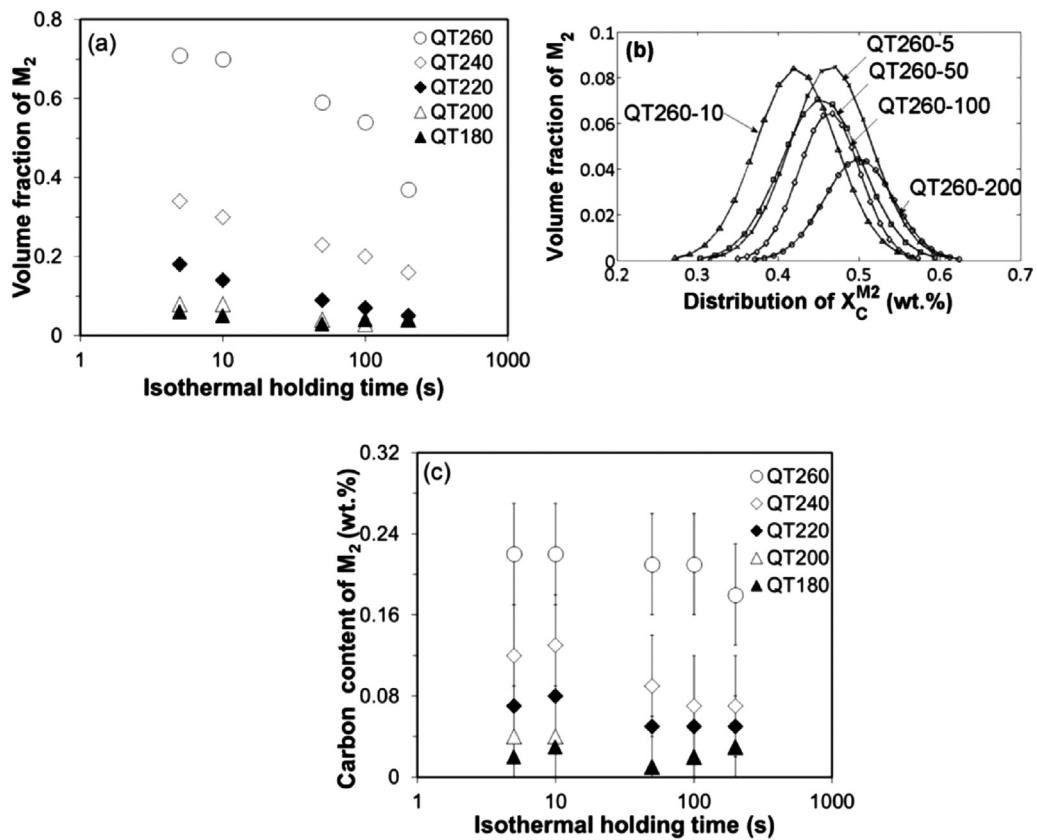

Fig. 9. The effect of the isothermal holding time on (a) volume fractions of M_2, (b) distribution of carbon in M_2 of the specimens QT260 and (c) total carbon content of M_2.

austenite. However, it might be that specimens are quenched before complete carbon homogenisation inside austenite grains has taken place. Moreover, in steels with inhomogeneous chemical composition (such as current study) the carbon concentration of unstable austenite decreases by moving from low-Mn regions to high-Mn regions. Low-Mn regions have higher fraction of M_1 than high-Mn regions, therefore unstable austenite in the low-Mn contains a higher carbon concentration. More details are given in Section 4.1. Note that the simulations procedure is simplified by assuming concentrations of substitutional elements as the nominal composition.

In order to analyse the unstable austenite with inhomogeneous carbon distribution, the unstable austenite is divided into subfractions with homogenous composition. This means that the

sum of the volume fractions i of unstable austenite with constant carbon concentration (f^i) is equal to the total fraction of unstable austenite (f^{UnSA}) as follows:

$$f^{UnSA} = \sum f^i \tag{4}$$

Accordingly, a combination of KM curves can simulate formation of M_2:

$$f^{M_2} = \sum_i f^i \left\{ 1 - \exp\left(-\alpha_m^i \left(T_{KM}^i - T \right) \right) \right\} \tag{5}$$

with α_m^i and T_{KM}^i as the KM parameters for segment i. The parameters α_m^i (K^{-1}) and T_{KM}^i (°C) depend on the chemical composition

[24] according to:

$$\alpha_m^i = 0.0224 - 0.0107X_C^i - 0.0007X_{Mn} - 0.00005X_{Ni}$$
$$- 0.00012X_{Cr} - 0.0001X_{Mo} \qquad (6)$$

$$T_{KM}^i = 462 - 273 X_C^i - 26X_{Mn} - 16X_{Ni} - 13X_{Cr} - 30X_{Mo} \qquad (7)$$

X_C^i (wt.%) is carbon concentration in the segment i of unstable austenite and X_j (wt.%) is concentration of element j (=Mn, Ni, etc.). Assuming that the carbon distribution follows a Gaussian function, the carbon distribution in M_2 can be determined by inserting Eq. (6) and Eq. (7) in Eq. (5) and considering the experimental plot of f^{M2} versus T. The Gaussian distribution of carbon is determined by three optimization variables: the peak height (f^i), position of the centre of the peak (μ) and the standard deviation (σ). The optimization problem is solved using "*MATLAB Optimization*" toolbox. According to Section 3. 3 austenite with carbon concentration higher than 1.2 wt.% is stable, thus the optimization problem has one constraints; the maximum carbon concentration of unstable austenite is 1.2 wt.%, i. e. $0 < \mu < 1.2$ wt.%, see section 3.3. Another constrain is that the total fraction of unstable austenite (f^{UnSA}) in Eq. (4) is given by $f^{UnSA} = f^{M2} = 1 - f^{M1} - f^B - f^{RA}$. Here, f^{RA} is considered as the volume fraction of stable austenite. Fig. 9b represents the carbon distribution in M_2 of the specimens QT260. During the isothermal holding, the Gaussian distribution of carbon moves toward higher concentrations, except when increasing the partitioning time from 5 s to 10 s. Similar tendency to move the Gaussian distribution of carbon toward higher concentrations is observed in the specimens QT220 and QT240. The carbon distributions in M_2 of the specimens QT180 and QT200 do not change significantly during the isothermal holding.

The total carbon content of M_2 (C^{M2}) can be determined by applying Eq. (2) as $C^{M2} = \sum_i f^i X_C^i$. Fig. 9c shows the influence of the isothermal holding time on C^{M2}. While C^{M2} of the specimens QT180 and QT200 is almost independent of the holding time, C^{M2} of the specimens QT220, QT240 and QT260 decreases after 50 s of isothermal holding. At constant isothermal holding time, C^{M2} increases by increasing the quenching temperature, however, increasing the quenching temperature from 180 °C to 200 °C does not influence C^{M2}.

3.7. Carbon content of initial martensite

Carbon in M_1 may precipitate as ε-carbide, segregate to defects or present in solid solution. The total carbon content of M_1 (C^{M_1}) can be determined by subtracting the carbon content of RA (C^{RA}) and the carbon content of M_2 (C^{M2}) from the carbon content of the steel (C) as:

$$C^{M_1} = C - C^{RA} - C^{M2} \qquad (8)$$

Due to the low carbon solubility in ferrite, the carbon content of carbide-free bainite is assumed zero. Considering the average carbon content of the steel (0.3 wt.%), C^{M_1} of the Q&P specimens were calculated with Eq. (8) and presented as a function of the isothermal holding time in Fig. 10. The time to reach a constant C^{M_1} is 5 s for the specimens QT220, QT240 and QT260. This time increases to 50 s for the specimens QT200 and QT180. For a constant partitioning time, C^{M_1} decreases by increasing the quenching temperature.
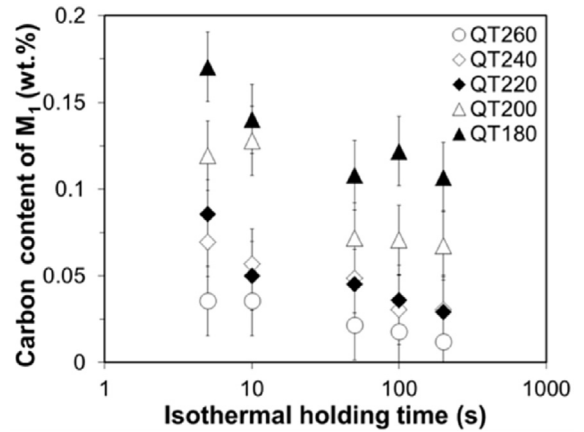

Fig. 10. The effect of isothermal holding on total carbon content of M_1 ($C^{M_1} = 0.3 - C^{M2} - C^{RA}$).

4. Discussion

4.1. Effect of the non-homogeneity of the chemical composition

According to Fig. 2a and b, higher fractions of M_1 are formed in low-alloying regions than high-alloying regions. This can be discussed on the basis of the relation between chemical composition and M_s [21], which is given in Eq. (1). Fig. 11 shows the influence of Mn and carbon segregation on M_s under two extreme conditions; (a) Mn concentration changes in the range of 2.90–4.20 wt.%, as it was measured by EPMA (Fig. 2b), and carbon concentration is constant (0.30 wt.%). (b) Carbon concentration changes between 0.29 and 0.31 wt.%, based on ThermoCalc calculations in Section 3.1, and Mn concentration is as nominal composition (3.50 wt.%). According to Fig. 11, while carbon segregation results in about 6 °C variations in M_s, Mn segregation leads to changes in M_s by about 61 °C. Here, Si concentration is taken as the nominal concentration (1.6 wt.%). Assuming carbon and Mn concentration as nominal composition of the steel, the measured Si segregation leads to about 7 °C changes in M_s. Consequently, the microstructural banding is mainly controlled by Mn segregation.

During the initial Q&P quenching, high-Mn regions, that are more stable than low-Mn regions, form lower fractions of M_1. Therefore, austenite in high-Mn regions has lower probability to receive sufficient carbon to remain at room temperature.
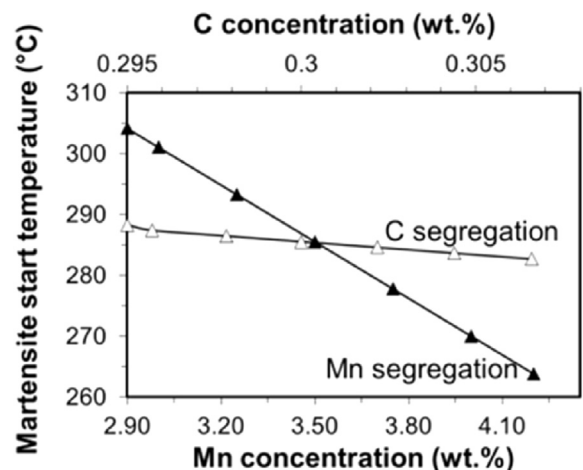

Fig. 11. The influence of Mn and carbon segregation on martensite start temperature.

Consequently, high-Mn regions have higher fractions of unstable austenite that transform to M_2 during the final quenching [25]. This explanation agrees well with Fig. 2a, in which higher fractions of M_2 are observed in high-Mn regions. It will be shown in Section 4.2 that unstable austenite may transform to bainite during isothermal holding. Accordingly, it is supposed that higher fractions of bainite form in high-Mn regions.

4.2. Influence of carbon partitioning on bainite formation

All Q&P specimens were isothermal held at the same temperature, therefore it is expected that the kinetics of bainite formation will be independent from quenching temperature. However, Fig. 8b shows that for a given isothermal holding time, the volume fraction of bainite is higher in the specimens quenched to higher temperature. This tendency could be related to the fact that specimens quenched to higher temperatures contain a higher fraction of austenite during isothermal holding. This implies that at constant isothermal holding time the normalised bainite fraction based on austenite fraction, i.e. ratio of volume fraction of bainite (f^b) to volume fraction of austenite ($f^a = 1 - f^{M_1}$), would be independent from quenching temperature. However, Fig. 12a shows that the ratio of f^b to f^a depends on the initial quenching temperature and is higher in the specimens quenched to higher temperature. Therefore, higher fraction of austenite in the specimens quenched to higher temperature is not the only reason of the increase of bainite formation by the increase of quenching temperature.

An alternative reason for the increase of bainite fraction by increasing the quenching temperature, is that specimens quenched

Fig. 12. (a) The normalised bainite fraction based on the volume fraction of austenite ($f^a = 1 - f^{M_1}$) as well as unstable austenite fraction ($f^{UnSA} = 1 - f^{M_1} - f^{SA}$) and (b) the kinetics of bainite formation (solid line) compared to the experimental data points (circles) for the specimens QT220, QT240 and QT260.

to higher temperature contain higher fraction of unstable austenite. This is based on the fact that at the beginning of isothermal holding, before bainite formation, some regions of austenite become stable via carbon partitioning process. Accordingly, austenite is divided to stable austenite, which does not decompose to bainite and is retained at room temperature, and unstable austenite, which may decompose to bainite. This assumption implies that the plot of normalised bainite fraction based on unstable austenite fraction (the ratio of f^b to volume fraction of unstable austenite ($f^{UnSA} = 1 - f^{M_1} - f^{SA}$)) versus isothermal holding time would be independent from the quenching temperature. Here, f^{SA} is assumed as f^{RA} after 5 s of isothermal holding, since there is a negligible bainite formation during this interval. Fig. 12a shows the ratio of f^B to f^{UnSA} is independent of quenching temperature. This confirms the initial assumption in which higher fraction of bainite in the specimen quenched to higher temperature is related to the higher fraction of unstable austenite.

The initial interfaces between martensite and unstable austenite act as potential sites of bainite nucleation [26]. However, it might be expected that the carbon partitioning leads to formation of a thin film of stable austenite, RA, in martensite-unstable austenite interfaces and therefore no bainite nucleates in these regions. This can be examined by observation of martensite-unstable austenite interfaces in EBSD micrograph of the specimen QT220-5 in Fig. 5. Note that here M_1–M_2 interfaces are considered as M_1-unstable austenite interfaces, since M_2 regions correspond to unstable austenite during the isothermal holding. As can be seen, there are M_1–M_2 interfaces that are free from RA and can be potential place of bainite nucleation. Note that some of austenite–austenite boundaries may be present in the microstructures, especially in specimens with high quenching temperature, that also act as bainite nucleation sites. However, such places have less density compared to martensite-unstable austenite and bainite–austenite interfaces and therefore they are not considered in the current calculations.

In this circumstance, the kinetics of bainite formation during isothermal holding of the Q&P process can be simulated on the basis of two points. First, the overall kinetics is controlled by the nucleation in both martensite-unstable austenite and bainite-–austenite interfaces. Second, stable austenite does not decompose to bainite. Under these assumptions, the kinetics of bainite formation is expressed based on the model developed in Ref. [27] as:

$$\frac{df^B}{dt} = \left(1 - f^B - f^{M1} - f^{RA}\right)\left(1 + \lambda^{M1} f^{M1} + \lambda^B f^B\right)\kappa \qquad (9)$$

in which λ^B and λ^{M1} are autocatalytic parameters of bainite nucleation at bainite-unstable austenite interfaces and martensite-unstable austenite interfaces, respectively. κ is a temperature dependent rate parameter and is given by Ref. [28]:

$$\kappa = \nu \frac{Z\delta}{D_A} \alpha_m exp\left(\frac{-K_1'}{R}\right)(T_h - T)exp\left(\frac{-Q_b}{RT}\right) \qquad (10)$$

where ν is the attempt frequency, δ is the effective thickness of the austenite grain boundary, Z is a geometrical factor, α_m is a kinetic parameter describing the rate of martensite formation and D_A is the parent austenite grain diameter. The parameter K_1 is a material constant and $1' = d(\Delta G_m)/dT$, i.e. the derivative of the maximum driving force ΔG_m with respect to temperature. In Eq. (10), K_1' (kJmol^{-1}K^{-1}) is given by (169.8 kJmol^{-1} – Q_b)/(705 K) and Q_b (kJmol^{-1}) can be calculated from Ref. [28]:

$$Q_b = 89\, X_C^{UnSA} + 10X_{Mn} + 12X_{Si} + 2X_{Cr} + 1X_{Ni} + 29X_{Mo} \qquad (11)$$
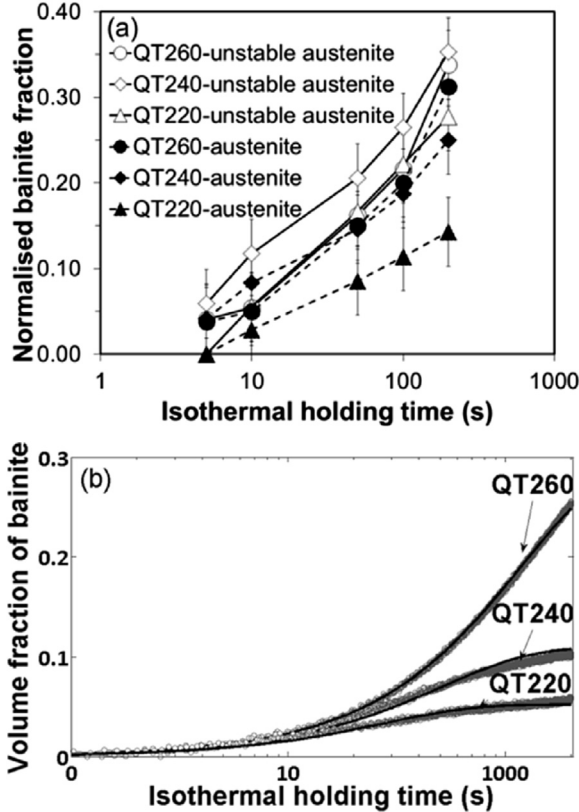
X_C^{UnSA} (wt.%) is the carbon concentration in unstable austenite and is assumed as the $X_C^{M_2}$ after 5 s of isothermal holding. The temperature T_h (°C) is the highest temperature at which a displacive transformation can occur and is given by Ref. [28]:

$$T_h = 835 - 198\, X_C^{UnSA} - 91 X_{Mn} - 15 X_{Si} - 73 X_{Cr} - 36 X_{Ni} - 87 X_{Mo} \tag{12}$$

The model is applied to simulate bainite formation in the specimen QT260-200. In the present study, $\nu = 10^{13}$ s^{-1}, $Z = 6$, $\delta = 1$ nm and $\alpha_m = 0.015$ K^{-1} [28] and D_A is estimated as 5 μm from SEM observation of the specimen QT260-5. Given that X_C^{UnSA} and f^{SA} are equal to $X_C^{M_2}$ and f^{M2}, the parameters are as estimated 0.45 wt.% and 0.06, respectively. Note that to simplify the calculation Mn and Si concentrations are assumed as the nominal composition. The autocatalysis coefficients are chosen 13 and 6 for austenite-martensite and austenite−bainite interfaces, respectively, for an optimum agreement between the model and the experimental fraction−time curve, as shown in Fig. 12b. Bainite formation during the isothermal holding of the specimens QT220 and QT240 is simulated, assuming that $\nu, Z, \delta, \alpha_m, D_A$, λ^B and λ^{M_1} are independent of the microstructure at the beginning of the isothermal holding. Fig. 12b shows that the model successfully simulates bainite formation in the specimens QT220 and QT240. For the specimens QT180 and QT200, in that most of austenite becomes stable after 5 s of isothermal holding, the simulations predict no bainite formation. This explains the insignificant fraction of bainite in these specimens.

4.3. Influence of carbon partitioning, bainite formation and carbide precipitation on the microstructure development

Presence of carbides in the SEM micrograph of the as-quenched specimen in Fig. 3a is due to auto-tempering of martensite during quenching. This process has been reported for steels with high M_s [29]. Therefore, ε-carbides which are in M$_1$, as detected in the TEM analysis of the specimen QT180-200 in Fig. 4c, are formed during the initial quenching. According to ThermoCalc calculations, ε-carbide is unstable at isothermal holding temperature (400 °C). Therefore, ε-carbide re-dissolves during this step and provides carbon for equilibrium cementite formation or for further carbon partitioning to austenite. Due to the slow kinetics of cementite formation in this high Si steel and fast kinetics of carbon partitioning from martensite [2], most of carbon partitions to austenite. Carbon depletion of martensite induces further decomposition of ε-carbide [30]. Regarding the fact that carbon from ε-carbide can partition to austenite after decomposition and in view of the slow kinetics of ε-carbide decomposition [30], long isothermal holding is required for complete carbon depletion of martensite. On the other hand, carbon partitioning simulations, in Section 3.3, show that all carbon in martensite diffuses to austenite within 1 s of isothermal holding. Note that the simulations assume that carbon in martensite is in solid solution. Therefore, carbon that remains in the microstructure after 1 s of isothermal holding can be assumed to be precipitated as ε-carbide or trapped at crystal. However, measurements of the carbon content of M$_1$ in the specimens QT180-5 and QT180-200, which were done by the authors by using 3D atom probe tomography [31], show that the concentration of solid solution carbon in M$_1$ in both specimens is about 0.05 wt.%. This indicates that most of carbon in M$_1$ precipitated as carbide. Therefore, the gradual decrease in carbon content of M$_1$ as a result of longer isothermal holding, that is observed in Fig. 10, is due to the decomposition of carbides and subsequent carbon partitioning.

Moreover, the carbon content of M$_1$ is higher in the specimens quenched to lower temperatures. The reason is that specimens quenched to lower temperatures have a higher fraction of M$_1$ and therefore a higher amount of carbon precipitates as carbide. Note that decomposition of ε-carbide during the isothermal holding (at 400 °C) of the current Q&P steel may seem contradictory with the observed formation of η-carbide in martensite during isothermal holding (at 400 °C) in a 0.38C-1.54Mn-1.48Si (wt.%) Q&P steel [32,33]. This apparent contradiction can be justified in view of the differences in the chemical composition of the steels, which influences the stability window of transition carbides. The stability of ε-carbide and η-carbide in these steels were calculated by using ThermoCalc. It should be recognized that at the initial stage of the isothermal holding carbon partitioning decreases the carbon content of martensite to a value lower than nominal concentration. Therefore, in the calculations the carbon concentration of each steel should be considered as the carbon concentration of martensite at the initial stage of the isothermal holding. This value was determined by applying Eq. (2) and inserting the total carbon content of M$_1$ (C^{M1}) and volume fraction of M$_1$ (f^{M1}) after 5 s and 10 s of isothermal holding for the current steel and the steel which was studied in Refs. [32,33], respectively. These isothermal holding times were the shortest reported times in each research. For the current study the calculation was limited to specimens quenched to 180 °C in which martensite had the highest carbon concentration among the other specimens. Considering that f^{M1} in the specimens QT180 is given as 0.8 in section 3.5 and C^{M1} in the specimen QT180-5 is 0.17 wt.% (Fig. 10), for the current research the carbon concentration of steel was given as 0.20 wt.%. Furthermore, the calculations for the steel studied in Refs. [32,33] were done by giving the carbon concentration of steel as 0.28 wt.%. This value was obtained under the assumption that C^{M1} is 0.25 wt.% (the total carbon content of martensite and η-carbide in Fig. 3c of [32]) and f^{M1} is 0.89 (remaining volume fraction after subtracting the volume fraction of RA from unity). According to the ThermoCalc calculations, there is a negligible temperature stability window for η-carbide in martensite in the current steel and therefore ε-carbide is the only transitional carbide. During the isothermal holding process, ε-carbide that was formed during initial quenching is unstable and re-dissolves. Due to the slow kinetics of cementite formation in this high Si steel and fast kinetics of carbon partitioning from martensite, most of carbon partitions to austenite. On the other hand, according to the ThermoCalc calculations of the steel of [32,33], at temperatures higher than 180 °C η-carbide is in metastable condition. Since the kinetics of formation of η-carbide is compatible with carbon partitioning, a fraction of carbon precipitates as η-carbide during the isothermal holding.

Simulations of carbon partitioning predicts that 200 °C is the optimum quenching temperature. As can be seen in Fig. 7a, the influence of isothermal holding on the calculated volume fractions of RA (f^{RA}) depends on whether the quenching temperature is above or below the optimum temperature. This agrees well with the calculations done in Ref. [34]. Increasing the isothermal holding time from 5 s to 200 s does not influence the simulated f^{RA} of the specimens quenched to the temperature equal or below the optimum temperature (specimens QT180 and QT200). In view of the small austenite grain size and regarding the fact that carbon partitioning is sufficient to stabilize all the austenite, austenite becomes stable within 5 s of isothermal holding and further tempering does not influence the microstructure. This is exemplified in Fig. 6a for the specimen QT180. For the specimens quenched to temperatures above the optimum temperature (specimens QT220, QT240 and QT260), the calculated f^{RA} decreases by increasing the isothermal holding time from 5 to 200 s. During 5 s−200 s of isothermal holding, carbon that was initially

accommodated near martensite-austenite boundaries becomes almost homogeneous inside the austenite grains. Due to the fact that the total amount of carbon is not sufficient to stabilize all austenite, homogenization of carbon inside austenite leads to a decrease on the fraction of stable austenite. The fact that after 5 s of isothermal holding the measured f^{RA} of specimens QT180, QT200 and QT220 is lower than the calculated ones can be related to the considerable degree of carbide precipitation in M_1 (Fig. 10). After 5 s of isothermal holding, the calculated and the measured f^{RA} of the specimens QT240 and QT260 are similar. This is due the fact that in these specimens a small fraction of carbon precipitated as carbide.

Increasing the isothermal holding time to 50 s increases the measured f^{RA} of the specimens QT180 and QT200 to values close to the simulated ones. This can be explained by the decomposition of some of ε-carbides and consequently carbon partitioning from M_1 to austenite. This agrees well with Fig. 10 which shows that C^{M1} decreases during 50 s of isothermal holding. Decomposition of ε-carbide and carbon partitioning from martensite during 50 s of isothermal holding also explains the increase of C^{RA} (Fig. 7c) and the decrease of f^{M_2} (Fig. 9a) of the specimens QT180 and QT200. Isothermal holding longer than 200 s does not significantly change the microstructure properties.

At isothermal holding times shorter than 5 s, there is a limited fraction of bainite in the specimens QT220, QT240 and QT260 (Fig. 8b). Therefore, in this time interval carbon partitioning from martensite to austenite controls the microstructure development. During isothermal holding longer than 5 s, carbide free-bainite forms in these specimens which is accompanied by carbon diffusion from bainitic ferrite to austenite. The steel contains a high concentration of Si and therefore it is supposed that carbide free-bainite is formed. In this regard, carbon diffusion from bainitic ferrite to austenite as well as carbon diffusion from martensite to austenite are responsible for the increase of measured f^{RA} (Fig. 7a) to the values higher than calculated ones, slighting the carbon distribution of M_2 toward higher concentration (Fig. 9b), the increase of C^{RA} of the specimens (Fig. 7c) and the decrease of volume fraction of M_2 (Fig. 9a). However, Fig. 10 shows that during 5 s–200 s of isothermal holding the amount of carbon partitioning from martensite is not significant and therefore carbon diffusion from bainitic ferrite is the prominent mechanism. It has worth to emphasize that in the current study bainite forms only from unstable austenite. In this matter, bainite formation decreases the fraction of unstable austenite (M_2) and does not decrease the fraction of stable austenite.

5. Conclusions

The interaction between carbon partitioning, carbide precipitation and carbide free bainite formation is studied during the application of the Q&P process to a 0.3C-1.6Si-3.5Mn (wt.%) steel with non-homogenous chemical composition. The main conclusions are:

1. Precipitation of ε-carbides during the first quenching reduces the amount of carbon in solid solution in martensite. Therefore the amount of carbon partitioning to the austenite is lower than according to simulations of carbon partitioning. Regarding the fact that the partitioning of carbon present in carbides requires the decomposition of the carbides and in view of slow kinetics of carbide decomposition, full completion of the carbon partitioning process can be achieved after isothermal holding time longer than predicted by simulations of carbon partitioning.
2. At the initial stage of isothermal holding, carbon partitioning stabilizes a certain fraction of austenite. This stable austenite does not decompose to bainite during the isothermal holding

and is retained at room temperature. In the specimens with lower quenching temperature, carbon partitioning stabilizes a higher fraction of austenite and therefore a lower fraction of bainite is formed.
3. Bainite formation reduces the volume fraction of secondary martensite, formed from unstable austenite, by two mechanisms. First, bainite formation is accompanied by carbon diffusion from bainite to austenite. This results in stabilization of a part of the unstable austenite. Second, bainite forms from unstable austenite and consequently decreases the fraction of unstable austenite.

References

[1] J.G. Speer, D.K. Matlock, B.C. De Cooman, J.G. Schroth, Carbon partitioning into austenite after martensite transformation, Acta Mater. 51 (2003) 2611–2622.
[2] D.V. Edmonds, K. He, F.C. Rizzo, B.C. De Cooman, D.K. Matlock, J.G. Speer, Quenching and partitioning martensite-A novel steel heat treatment, Mater. Sci. Eng. A 438–440 (2006) 25–34.
[3] F. HajyAkbary, M.J. Santofimia, J. Sietsma, Optimizing mechanical properties of a 0.3C-1.5Si-3.5Mn quenched and partitioned steel, Adv. Mater. Res. 829 (2014) 100–104.
[4] J.G. Speer, F.C. Rizzo, D.K. Matlock, D.V. Edmonds, The "quenching and partitioning" process: background and recent progress, Mater. Res. 8 (2005) 417–423.
[5] J.G. Speer, D.K. Matlock, B.C. De Cooman, J.G. Schroth, Comments on "On the definitions of paraequilibrium and orthoequilibrium by M. Hillert and J. Ågren, Scripta Materialia, 50, 697–9 (2004)", Scr. Mater. 52 (2005) 83–85.
[6] M.J. Santofimia, L. Zhao, J. Sietsma, Model for the interaction between interface migration and carbon diffusion during annealing of martensite–austenite microstructures in steels, Scr. Mater. 59 (2008) 159–162.
[7] M.J. Santofimia, L. Zhao, J. Sietsma, Microstructural evolution of a low-carbon steel during application of quenching and partitioning heat treatments after partial austenitization, Metall. Mater. Trans. A 40 (2009) 46–57.
[8] H.K.D.H. Bhadeshia, D.V. Edmonds, The bainite transformation in a silicon steel, Metall. Trans. A 10 (1979) 895–907.
[9] E.J. Seo, L. Cho, B.C. De Cooman, Application of quenching and partitioning (Q&P) processing to press hardening steel, Metall. Mater. Trans. A 45 (2014) 4022–4037.
[10] J. Mola, B.C. De Cooman, Quenching and partitioning (Q&P) processing of martensitic stainless steels, Metall. Mater. Trans. A 44 (2013) 946–967.
[11] Y. Toji, G. Miyamoto, D. Raabe, Carbon partitioning during quenching and partitioning heat treatment accompanied by carbide precipitation, Acta Mater. 86 (2015) 137–147.
[12] J.G. Speer, A.M. Streicher, D.K. Matlock, F.C. Rizzo, G. Krauss, Quenching and partitioning: A fundamentally new process to create high strength trip sheet microstructures, in: Materials Science and Technology Meeting, 2003. Chicago, IL; United States.
[13] J.H. Jang, I.G. Kim, H.K.D.H. Bhadeshia, ε-Carbide in alloy steels: first –principles assessment, Scr. Mater. 63 (2010) 121–123.
[14] W.M. Garrison Jr., Ultra-strength steels for aerospace applications, J. Minerals, Metals Mater. Soc. (TMS) 42 (1990) 20–24.
[15] M.J. Santofimia, L. Zhao, R. Petrov, C. Kwakernaak, W.G. Sloof, J. Sietsma, Microstructural development during the quenching and partitioning process in a newly designed low-carbon steel, Acta Mater. 59 (2011) 6059–6068.
[16] M.J. Duggin, Thermally induced phase transformations in iron carbides, Trans. Met. Soc. AIME 242 (1968) 1091–1100.
[17] E.J. Fasiska, G.A. Jeffrey, On the cementite structure, Acta Cryst. 19 (1965) 463–471.
[18] M.J. Santofimia, R. Petrov, L. Zhao, J. Sietsma, Microstructural analysis of martensite constituents in quenching and partitioning steels, Mater. Charact. 92 (2014) 91–95.
[19] T. Swarr, G. Krauss, The effect of structure on the deformation of as-quenched and tempered martensite in an Fe-0.2 pct C alloy, Metall. Trans. A 7 (1976) 41–48.
[20] A. J. Clarke, Ph.D. Thesis, 2006: Colorado School of Mines, pp. 31–32.
[21] S.M.C. van Bohemen, Bainite and martensite start temperature calculated with exponential carbon dependence, Mater. Sci. Technol. 28 (2012) 487–495.
[22] M.J. Santofimia, L. Zhao, J. Sietsma, Volume change associated to carbon partitioning from martensite to austenite, Mater. Sci. Forum 706–709 (2012) 2290–2295.

[23] D.P. Koistinen, R.E. Marburger, A general equation prescribing the extent of the austenite-martensite transformation in pure iron-carbon alloys and plain carbon steels, Acta Metal. 7 (1959) 59–60.

[24] S.M.C. van Bohemen, J. Sietsma, Martensite formation in partially and fully austenitic plain carbon steels, Metall. Mater. Trans. A 40 (2009) 1059–1068.

[25] F. HajyAkbary, C. Kwakernaak, R.H. Petrov, G. Miyamoto, T. Furuhara, J. Sietsma, M.J. Santofimia, Effect of Mn segregation on the microstructure development of Q&P steels, in: International Conference on Solid-solid Phase Transformations in Inorganic Materials (PTM), Canada, 2015.

[26] M.J. Santofimia, S.M.C. van Bohemen, D.N. Hanlon, L. Zhao, J. Sietsma, Perspectives in high-strength steels: interactions between non-equilibrium phases, in: Intl. Symp. On New Developments in Advanced High-strength Sheet Steels, 2013.

[27] S.M.C. van Bohemen, D.N. Hanlon, A physically based approach to model the incomplete bainitic transformation in high-Si steels, Int. J. Mater. Res. 103 (2012) 987–991.

[28] S.M.C. van Bohemen, Modeling start curves of bainite formation, Metall. Mater. Trans. A 41 (2010) 285–296.

[29] G.R. Speich, W.C. Leslie, Tempering of steel, Metall. Trans. A 3 (1972) 1043–1054.

[30] J. Gordine, I. Codd, The influence of Si up to 1.5 wt% on the tempering of a spring steel, J. Iron Steel Inst. 207 (1969) 461–467.

[31] F. HajyAkbary, M. J. Santofimia G. Miyamoto, N. Kamikawa, T. Furuhara, R. H. Petrov and J. Sietsma, Analysis of the Mechanical Behavior of a 0.3C-1.6Si-3.5Mn (wt.%) Quenching and Partitioning Steel, (to be published).

[32] D.T. Pierce, D.R. Coughlin, D.L. Williamson, K.D. Clarke, A.J. Clarke, J.G. Speer, D.K. Matlock, E. De Moor, Mössbauer spectroscropy investigation of transition carbides in quenched and partitioned steel, in: International Conference on Solid-solid Phase Transformations in Inorganic Materials (PTM), Canada, 2015.

[33] D.T. Pierce, D.R. Coughlin, D.L. Williamson, K.D. Clarke, A.J. Clarke, J.G. Speer, E. De Moor, Characterization of transition carbides in quench and partitioned steel microstructures by Mössbauer spectroscopy and complementary techniques, Acta Mater. 90 (2015) 417–430.

[34] A.J. Clarke, J.G. Speer, M.K. Miller, R.E. Hackenberg, D.V. Edmonds, D.K. Matlock, F.C. Rizzo, K.D. Clarke, E. De Moor, Carbon partitioning to austenite from martensite or bainite during the quench and partition (Q&P) process: A critical assessment, Acta Mater. 56 (2008) 16–22.